Characterization of aerosol hygroscopicity, mixing state, and CCN activity at a suburban site in the central North China Plain

Yuying Wang[1], Zhanqing Li[1], Yingjie Zhang[2], Wei Du[2,3], Fang Zhang[1] , Haobo Tan[4], Hanbing Xu[5], Tianyi Fan[1], Xiaoai Jin[1], Xinxin Fan[1], Zipeng Dong[1], Qiuyan Wang[6], Yele Sun[2,3]

[1]College of Global Change and Earth System Science, Beijing Normal University, Beijing 100875, China

[2]State Key Laboratory of Atmospheric Boundary Layer Physics and Atmospheric Chemistry, Institute of Atmospheric Physics, Chinese Academy of Sciences, Beijing 100029, China

[3]College of Earth Sciences, University of Chinese Academy of Sciences, Beijing 100049, China

[4]Key Laboratory of Regional Numerical Weather Prediction, Institute of Tropical and Marine Meteorology, China Meteorological Administration, Guangzhou 510080, China

[5]Shared Experimental Education Center, Sun Yat-sen University, Guangzhou 510275, China

[6]Collaborative Innovation Center on Forecast and Evaluation of Meteorological Disasters, Nanjing University of Information Science and Technology, Nanjing, 210044, China

**Correspondence to*: Zhanqing Li (zli@atmos.umd.edu)

Abstract. Aerosol hygroscopicity, mixing state and CCN activity were investigated as a part of the Atmosphere-Aerosol-Boundary Layer-Cloud (A^2BC) Interaction Joint Experiment carried out at Xingtai (XT), a suburban site in the center of the North China Plain (NCP). In general, the probability density function of the hygroscopicity parameter (κ-PDF) for 40–200 nm particles had a unimodal distribution and mean κ-PDF patterns for different sizes were similar, suggesting that the particles were highly aged and internally mixed because of strong photochemical reactions. The κ calculated from hygroscopic growth factor in the daytime and at nighttime showed that photochemical reactions largely enhanced the aerosol hygroscopicity, and the effect became weaker as the particle size increased. In addition, the aerosol hygroscopicity was much larger at XT than at sites in the northern part of the NCP, illustrating that the hygroscopicity of particles varies largely due to different emissions and chemical processes in the NCP.

Measurement results also showed that new particle formation events occurred frequently at XT, one of the most polluted city in China. The evolution of the planetary boundary layer played a dominant role in aerosol mass concentration changes while particle formation and growth had a greater influence on the variation in aerosol number concentrations. Particle size was the most important factor influencing the ability of aerosols to activate, especially at higher levels of supersaturation (SS). The cloud condensation nuclei (CCN) number concentration (N_{CCN}) derived from chemical composition was highly correlated with the measured N_{CCN} ($R^2 \geqslant 0.85$), but was generally overestimated due to measurement uncertainties.

The effect of chemical composition on N_{CCN} was weaker relative to the particle size. N_{CCN} sensitivity tests showed that the impact of chemical composition on N_{CCN} became weaker with increasing SS, suggesting that chemical composition played a less role in N_{CCN} estimations at higher SS levels. A good proxy for the chemical comical composition (κ = 0.31) was found, which can simplify the calculation of N_{CCN} on models.

1. Introduction

Aerosols, defined as the mixture of solid and liquid particles suspended in air, are ubiquitously present in the atmosphere because of direct emissions from biogenic and anthropogenic sources and the secondary transformation from gas precursors. Aerosol particles play an important role in climate changes through direct and indirect effects (e.g. Ramanathan et al., 2001; Daniel et al., 2008; Li et al., 2016). However, the impact of aerosols on climate change is difficult to simulate because of the highly variable physical and chemical properties of aerosols, and complex aerosol-cloud interactions (IPCC, 2013; Lebo et al., 2017).

The hygroscopic growth and mixing state of aerosol particles are important for estimating the direct climate effect of aerosols. This is because the growth and mixing can change the particle size and optical properties of aerosol particles, directly influencing the terrestrial radiation budget and degrading the atmospheric visibility (e.g. Covert et al., 1972; Stock et al., 2011; Peng et al., 2016; Z. Li et al., 2017). In addition, aerosol particles can be activated as cloud condensation nuclei (CCN) under supersaturation (SS) conditions. The variability in CCN number concentration (N_{CCN}) can modify cloud microphysical properties, thereby causing an indirect radiative forcing (Twomey, 1974; Albrecht, 1989). Previous studies have addressed three main aerosol properties influencing the CCN activation, namely, particle size, chemical composition, and mixing state. However, their relative importance is different in different environments (e.g. Dusek et al., 2006; Ervens et al., 2007; Cubison et al., 2008; Deng et al., 2011; Zhang et al., 2014; Schmale et al., 2018).

Ambient aerosols are composed of different species, including inorganic ions, organic components, black carbon (BC), and mineral dust. Inorganics mainly contain sulfate, nitrate, and ammonium, while organic aerosols (OA) consist of thousands of chemicals (Jacobson et al., 2000). The hygroscopicity and CCN activity of a single component can be characterized according to laboratory studies (e.g. Petters and Kreidenweis, 2007), but the properties of their mixtures are hard to estimate because of the different chemical species and mixing states of particles in the atmosphere. Therefore, aerosol hygroscopicity and CCN activity are very different in different regions due to different chemical compositions. Comprehensive field measurements of aerosol properties in different areas are necessary to improve models.

China, especially the North China Plain (NCP), has been suffered from severe air pollution since its rapid industrialization and urbanization in the last couple of decades, where diverse sources and aging processes make aerosol properties particularly diverse and complex. As such, the region has drawn much attention in studying the aerosol mixing state, hygroscopicity, and CCN activity (Deng et al., 2011;

Liu et al., 2011; Zhang et al., 2014; F. Zhang et al., 2016; S.L. Zhang et al., 2016; Wu et al., 2016; Y. Wang et al., 2017). Liu et al. (2011) and Y. Wang et al. (2017) have suggested that ambient particles are mostly an external mixture with different hygroscopicities. Deng et al. (2011) has shown that the aerosol number size distribution is critical in the prediction of N_{CCN} while Zhang et al. (2014, 2017) have highlighted the importance of chemical composition in determining particle activation properties. However, all these studies were done using data from the northern part of the NCP. Few studies have focused on the central region of the NCP. Compared to the northern part of the NCP, the central part of the NCP is more affected by industrial emissions where a dense cluster of China's heavy industries exist (Fu et al., 2014). Measurement of aerosol properties in the central part of the NCP are critically needed to investigate the impact of air pollution on the environment and climate changes.

Xingtai (XT), a city located in the central area of the NCP, often ranks in the top of polluted cities in China. Local industrial and domestic sources are the greatest contributors to severe haze events (Wang et al., 2014). A field experiment called the Atmosphere-Aerosol-Boundary Layer-Cloud (A^2BC) Interaction Joint Experiment was carried out at a suburban site in Xingtai in the summer of 2016. Differences in aerosol properties at this site and at sites in the northern part of the NCP were found in this study.

The paper is organized as follows. Sections 2 and 3 describe the measurement method and data analysis theory. Section 4 presents and discusses the measurement results, which includes the data time series, aerosol mixing state, hygroscopicity, CCN prediction and its sensitivity to chemical composition. A summary and conclusions are given in section 5.

2. Measurements

2.1. Sampling site and meteorology

The A^2BC was carried out at the National Meteorological Basic Station located in XT (37.18° N, 114.37° E, 180 m ASL) from 1 May to 15 June of 2016. This suburban site is situated ~ 17 km northwest of Xingtai urban area in southern Heibei Province, located in the central part of the NCP and to the east of Taihang Mountains (Fig. 1a). This region is heavily populated, urbanized, and industrialized. The major industrial manufacturers include coal-based power plants, steel and iron works, glassworks, and cement mills. The weak diffusion conditions and heavy industrial emissions lead to exceptionally high concentrations of particulate matter (PM) with diameter less than 10 μm (PM_{10}) and 2.5 μm ($PM_{2.5}$), as well as gas pollutants such as sulfur dioxide (SO_2), volatile organic compounds (VOCs) and nitrogen oxides (NO_x) during the frequent occurring haze episodes in this region (Wang et al., 2014; Fu et al., 2014). Figure 1b shows the mean distribution of SO_2 concentrations from May of 2012 to 2016, confirming that the measurement site is located in one of the pollution centers in this region. The detailed analysis of gas precursors and aerosol chemical species shows this station is a good representative site in this region (Zhang et al., 2018).

Time series of meteorological variables measured at this meteorological station are shown in Fig. S1. This site is heavily affected by the mountain-valley wind, showing a prevailing southeasterly wind during the day and a northwesterly wind at night (Fig. S1 and Fig. S2). There was almost no precipitation during the study period. The ambient temperature (*T*) and relative humidity (RH) time series show opposing trends. Campaign-mean values of *T* and RH are 21.9 ºC and 51.6 %, respectively.

2.2. Instrumentation and operation

2.2.1. Aerosol hygroscopicity measurements

The custom-built hygroscopicity tandem differential mobility analyzer (H-TDMA) used in this study has been described in detail by others (Tan et al., 2013; Y. Wang et al., 2017). Briefly, ambient aerosols are first dried and neutralized by a Nafion dryer and a soft X-ray charger. A differential mobility analyzer (DMA_1, model 3081L, TSI Inc.) is used to select monodispersed particles of a certain diameter (D_{p0}). The monodisperses particles are then pass through a nafion humidifier with a controlled higher RH and are humidified. A second DMA (DMA_2, same model as the DMA_1) and a water-based condensation particle counter (WCPC, model 3787, TSI Inc.) are used to measure the number size distribution of the humidified particles. The DMA_1 and WCPC can also be connected directly to measure the 10–400 nm particle number size distribution (PNSD). In this study, the dry diameters selected by the DMA_1 are 40, 80, 110, 150, and 200 nm. The humidified RH is set to 85 %, the RH calibration with ammonium sulfate for the HTDMA is shown in Fig. S3 in the supplement.

The hygroscopic growth factor (GF) is defined as the ratio of the humidified diameter at a given RH to the dry diameter:

$$\mathrm{GF} = \frac{D_\mathrm{p}(\mathrm{RH})}{D_\mathrm{po}}, \quad (1)$$

where $D_\mathrm{p}(\mathrm{RH})$ is the particle diameter at the given RH and D_p0 is the dry diameter selected by the DMA_1. The measured distribution function versus GF (GF-MDF) can be calculated with WCPC data downstream from the DMA_1 and DMA_2. The GF probability density function (GF-PDF) is then retrieved using the TDMAFIT algorithm (Stolzenburg and McMurry, 1988, 2008).

2.2.2. Aerosol chemical composition measurements

An Aerosol Chemical Speciation Monitor (ACSM) was deployed to measure the non-refractory submicron aerosol (NR-PM_1) species (sulfate, nitrate, ammonium, chloride, and organics) in real-time. A $\mathrm{PM}_{2.5}$ URG cyclone (model URG-2000-30ED) was installed in the front of the sampling inlet to remove coarse particles (> 2.5 μm in diameter). Before sampling into the ACSM, aerosol particles were dried (below 40 % RH) by a silica gel diffusion dryer. In addition, the ACSM was calibrated routinely with pure ammonium nitrate to determine its ionization efficiency. More detailed descriptions about the ACSM are given by Ng et al., (2011) and Sun et al., (2012). A positive matrix factor analysis is used to analyze the organic spectral matrices according to Ulbrich et al., (2009). Three factors, i.e., hydrocarbon-like OA (HOA), cooking OA (COA), and oxygenated OA (OOA), are chosen as the ACSM dataset. HOA and COA are both primary organic aerosols (POA) while OOA is the secondary organic aerosol (SOA).

The ACSM does not detect refractory material such as BC, so a seven-wavelength aethalometer (AE-33, Magee Scientific Corp.) was used to measure the BC mass concentration of BC particles with diameters < 1.0 μm (BC PM_1). Mineral dust and sea salt are the other refractory species, but they typically exist in the coarse mode and make negligible contributions to PM_1 (Juranyi et al., 2010; Meng et al., 2014).

2.2.3. Aerosol size distribution and CCN measurements

The aerosol particle number size distribution (15–685 nm) was measured by a scanning mobility particle sizer (SMPS) that was equipped with a long DMA (model 3081L, TSI Inc.) and a condensation particle counter (CPC, model 3775, TSI Inc.). A single-column continuous-flow thermal-gradient cloud condensation nuclei counter (CCNC-100, DMT Inc.) was applied to measure the bulk CCN number concentration. Five SS levels, i.e., 0.07, 0.1, 0.2, 0.4, and 0.8 %, were set in the CCNC and the running time was 10 min for each SS level. The SS in the CCNC were calibrated with pure ammonium sulfate (Rose et al., 2008) before and after the measurement campaign. The corrected SS levels were 0.11, 0.13, 0.22, 0.40, and 0.75 %, respectively.

The aerosol activation ratio (AR) at a certain SS is calculated as N_{CCN} divided by the total particle number concentration in the 15–685 nm range ($N_{15\text{–}685\,\mathrm{nm}}$), i.e., AR = $N_{\mathrm{CCN}} / N_{15\text{–}685\,\mathrm{nm}}$. The particle number concentration below 15 nm is not measured by the SMPS, but this does not affect the calculated N_{CCN} because the activation critical diameter is always larger than 15 nm at these SS levels (Zhang et al., 2014). Aerosol particles with diameters larger than 685 nm are also not detected by the SMPS. These larger particles will always act as CCN due to their larger dry sizes. However, the number concentration above 685 nm in the atmosphere is always negligible (Juranyi et al., 2010).

2.2.4. Other measurements

In this study, a micro-pulse lidar (MPL-4B, Sigmaspace Corp.) was used to study the evolution of the planetary boundary layer (PBL). The pulse repetition rate of the MPL was 2.5 kHz at a visible wavelength of 532 nm. The peak value of the optical energy of the laser beam was 8 μJ. The pulse duration ranged from 10 to 100 ns, and the pulse interval was set to 200 ns, corresponding to a spatial resolution of 30 m. The MPL-retrieved PBL height is the altitude where a sudden decrease in the scattering coefficient occurs (Brooks, 2003; Quan et al., 2013). Trace gas analyzers (manufactured by ECOTECH) were used to measure the gaseous species of O_3, SO_2, NOx, NO and CO. More detailed descriptions about the analyzers are given by Zhu et al., (2016).

During this campaign, all sampling instruments were placed in two containers at ground level and two air conditioners were used to maintain the temperature at 20–25 °C inside containers. All stainless tube inlets were ~ 1.5 m above the top of containers.

3. Theory

3.1. Hygroscopicity parameter

To link hygroscopicity measurements below and above water vapor saturation, the Köhler theory (Köhler, 1936) is parameterized using the hygroscopicity parameter κ (Petters and Kreidenweis, 2007). This is known as the κ-Köhler theory. According to the theory, the equilibrium equation over a solution droplet at a saturation ratio $S(D)$ is

$$S(D) = \frac{D^3 - D_d^3}{D^3 - D_d^3(1-\kappa)} \exp\left(\frac{4\sigma_{\mathrm{s/a}} M_{\mathrm{w}}}{RT\rho_{\mathrm{w}} D}\right) \quad , \tag{2}$$

where D and D_d are the wet and dry droplet diameters, respectively, $\sigma_{\mathrm{s/a}}$ is the surface tension coefficient, M_{w} is the mole mass of water, R is the universal gas constant, T is the temperature, and ρ_{w} is the density of water.

Below the water vapor saturation, $S(D)$ is RH, D is $D_{\mathrm{p}}(\mathrm{RH})$, and D_d is D_{p0} in Eq. (1). The κ parameter is then calculated using H-TDMA data according to Eq. (1) and Eq. (2):

$$\kappa_{\mathrm{gf}} = (\mathrm{GF}^3 - 1) \cdot \left[\frac{1}{\mathrm{RH}} \exp\left(\frac{4\sigma_{\mathrm{s/a}} M_{\mathrm{w}}}{RT\rho_{\mathrm{w}} D_d \mathrm{GF}}\right) - 1\right] \quad . \tag{3}$$

For a multicomponent particle, the Zdanovskii–Stokes–Robinson (ZSR) mixing rule (Stokes and Robinson, 1966) can also estimate κ using chemical composition data:

$$\kappa_{\mathrm{chem}} = \sum_i \varepsilon_i \kappa_i, \tag{4}$$

where ε_i and κ_i are the volume fraction and hygroscopicity parameter for the ith chemical component. The ACSM provides the mass concentrations of inorganic ions and organics. A simplified ion-pairing scheme such as that described by Gysel et al. (2007) is applied to convert ion mass concentrations to mass concentrations of their corresponding inorganic salts (see Table S1 in the supplement). Table S1 also lists κ and the gravimetric density of each individual component under supersaturated conditions. In the following discussions, κ_{gf} and κ_{chem} denote the hygroscopicity parameters derived from H-TDMA measurements and estimated using the ZSR mixing rule, respectively.

3.2. CCN estimation

The critical supersaturation (s_c, $s_c = S_c$-1) for a dry diameter (D_d) of a particle with hygroscopicity κ is calculated from the maximum of the κ-Köhler curve (Eq. 2) (Petters and Kreidenweis, 2007). The D_d is also the critical diameter corresponding to the s_c when κ is known, so the s_c-D_d relationship can be established. According to this relationship, the critical diameter ($D_{0,\mathrm{crit}}$) can be calculated using the estimated κ_{chem} (Eq. 4) at a given SS. All particles larger than $D_{0,\mathrm{crit}}$ will activate as CCN, assuming that aerosols are internally mixed. Then the CCN number concentration can be estimated from the integral of the aerosol size distribution provided by the SMPS from $D_{0,\mathrm{crit}}$ to the maximum measured size (D_{max}) following Eq. (5):

$$N_{\mathrm{CCN}}(\mathrm{SS}) = \int_{D_{0,\mathrm{crit(SS)}}}^{D_{\mathrm{max}}} \frac{dN(D)}{d\log(D)} d\log(D) \qquad (5)$$

$N_{\mathrm{CCN}}(\mathrm{SS})$ can then be compared to the number of CCN at the same SS measured by the CCNC (i.e. a closure study).

4. Results and discussion

4.1. Overview

Figures 2 and 3 show the time series of the main aerosol properties during the this campaign. The PNSD changes dramatically (Fig. 2a) and the aerosol number concentration in the 15–50 nm range ($N_{15\text{–}50\ \mathrm{nm}}$) increases sharply in the morning almost every day (Fig. 2b). The time series of the mean diameter (D_m) of particles also shows that a growth process occurs after the sharp increase in $N_{15\text{–}50\ \mathrm{nm}}$. All these phenomena suggest that new particle formation (NPF) events occurred frequently at XT during the field experiment (Kulmala et al., 2012; Y. Li et al., 2017). This is likely related to the high concentration of gas precursors mainly from local emissions. High emissions of SO_2 and volatile organic compounds (VOCs) associated with the high oxidation capacity in a polluted atmosphere make NPF events occur more frequently in north China (Z. Wang et al., 2017).

Figure 2c-d shows the time series of the probability density function of κ_{gf} (κ-PDF) for 40 nm and 150 nm particles, respectively. In general, mono-modal κ-PDFs were observed. This is different from κ-PDFs at other sites in China where bi- and tri-modal distributions are dominant (Liu et al., 2011; Ye et al., 2013; Jiang et al., 2016; S.L. Zhang et al., 2016; Y. Wang et al., 2017). This is due to differences in the aerosol mixing state, which will be discussed in section 4.2.

The bulk mass concentrations of organics, sulfate, nitrate, ammonium, and chloride measured by the ACSM are shown in Fig. 3a, along with the BC mass concentration measured with the AE-33. Organics and sulfate were the dominant chemical species with mass fractions in PM_1 of 39.1 % and 24.7 %, respectively. Figure 3b-c shows the volume fractions of paired chemical compositions and the hygroscopicity parameter (κ_{chem}) derived from chemical compositions, respectively. The average volume fraction of inorganics ($(NH_4)_2SO_4$+NH_4HSO_4+H_2SO_4+NH_4NO_4) was similar to that of organics (POA+SOA), but their volume fractions changed diurnally. In general, the volume fraction of inorganics increased during daytime while the volume fraction of organics decreased. In addition, SOA was the dominant contributor to OA, accounting for ~69 % of the organics volume. This shows that photochemical reactions were strong at XT during this campaign (Huang et al., 2014). The mean κ_{chem} in Fig. 3c was 0.31 with values ranging from 0.20 to 0.40. The trend in κ_{chem} was similar to that of the volume fraction of inorganics, suggesting that inorganics plays a key role when it comes to κ_{chem}, this is consistent with the study of Wu et al. (2016).

4.2. Aerosol mixing state and hygroscopicity

The average probability density functions of κ_{gf} (κ-PDF) for different particle sizes derived from H-TDMA data are shown in Fig. 4. For all particle sizes considered, κ_{gf} ranged from 0 to 0.8 and the κ-PDF patterns were similar, suggesting that the hygroscopic compounds in different particle size mode were similar at XT. In general, κ-PDF patterns show only one hydrophilic mode with the weak hydrophobic mode occasionally appearing at night when photochemical reactions are weak (Fig. S4).

This is different from what has been reported at other sites in China (Liu et al., 2011; Ye et al., 2013; Jiang et al., 2016; Zhang et al., 2016; Y. Wang et al., 2017) where the κ-PDF patterns always show bi- or tri-modal distributions. Based on previous studies (Liu et al., 2011; Y. Wang et al., 2017), ambient aerosols can be classified into three groups according to their κ_{gf} values:

- nearly hydrophobic (NH): $\kappa_{\mathrm{gf}} < 0.1$
- less hygroscopic (LH): $0.1 \leqslant \kappa_{\mathrm{gf}} < 0.2$
- more hygroscopic (MH): $0.2 \leqslant \kappa_{\mathrm{gf}}$

Table 1 gives the number fractions of each group for different particle sizes. The MH group dominated all particle sizes. The number fractions of the NH and LH groups were less than 6.0 % each. However, the volume fractions of hydrophobic BC and low-hygroscopic organics (where κ_{BC} is approximately zero and $\kappa_{\mathrm{organic}}$ is typically less than 0.1) were ~10.1 % and 47.4 % according to chemical composition measurements (Fig. 3b). This suggests that the particles were highly aged and internally mixed at XT during this campaign. Coating of sulfates and secondary organics during the aging process changes the structure of BC and makes it grow, which can significantly enhance the hygroscopicity of particles (e.g., Zhang et al., 2008; Jimenez et al., 2009; Tritscher et al., 2011; Guo et al., 2016). In addition, the observed unimodal distribution of κ-PDF also suggests the internal mixing state of the particles (Swietlicki et al., 2008).

Figure 5 shows the average size-resolved κ_{gf} derived from H-TDMA data at XT and at other sites in China. At XT, κ_{gf} for different particle sizes were larger in the daytime than at night and the difference between daytime and nighttime decreased with increasing particle size. This suggests that the impact of photochemical reactions on aerosol hygroscopicity is strong and that the effect is weaker with increasing particle size because most of the larger particles are always well aged.

The magnitude of κ_{gf} was larger at XT than at other sites of China. In particular, the magnitude of κ_{gf} was much larger at XT than at sites in the northern part of the NCP, i.e., Beijing, Wuqing, and Xianghe. The lower κ_{gf} in the urban area of Beijing is likely related to the more severe traffic emissions (Ye et al., 2013; Wu et al., 2016). Wuqing and Xianghe are located in the suburban area between the two megacities of Beijing and Tianjin and are simultaneously affected by traffic and industrial emissions. The magnitude of κ_{gf} at these two sites are higher than at Beijing but lower than at XT. Although XT is located far away from these megacities, it is situated in the industrial center of the NCP, so the higher concentrations of precursors and strong photo chemical reactions make the particles more internally mixed and highly aged. This is why κ_{gf} in XT is larger than at other sites. This suggests that the hygroscopicity of particles from different emissions and chemical processes differ in NCP. In addition, 40 nm particles were always more hygroscopic than 80 nm particles at XT, especially in the daytime, which was also different from other sites. This is likely because the coating effect of sulfates and secondary organics is more significant on smaller particles (Tritscher et al., 2011; Guo et al., 2016). Furthermore, since the field measurements took place in a local with heavy industrial activities, it is possible that amine contributes significantly to the hygroscopicity of 40 nm particles. Several studies have shown that amine compounds in aerosol phase can be hygroscopic, sometimes at even low RH (e.g. Qiu and Zhang, 2012; Chu et al., 2015; Gomez-Hernandez et al., 2016).

4.3. Diurnal variations in aerosol properties

4.3.1. Diurnal variations in aerosol number and mass concentrations

Figure 6a shows the diurnal variation in MPL-derived PBL height. PBL height can be determined at the altitude where a sudden decrease in the scattering coefficient occurs from the MPL data (Cohn and Angevine, 2000; Brooks, 2003). Note that the retrieved PBL height is only valid from 07:00 local time (LT) to 19:00 LT (Quan et al., 2013). The retrieved PBL height at night is not accurate because of the likely influence of residual aerosols within the nocturnal PBL. The evolution of PBL height from 07:00 LT to 19:00 LT is sufficient to analyze its link with the change in aerosol number and mass concentrations during the daytime. Figure 6b shows diurnal variations in aerosol number and mass concentrations in the 15–685 nm range ($N_{15–685\ \mathrm{nm}}$ and $\mathrm{PM}_{15–685\ \mathrm{nm}}$, respectively). Variations in the $N_{15–685\ \mathrm{nm}}$ and $\mathrm{PM}_{15–685\ \mathrm{nm}}$ trended oppose each other. From 08:00 LT to 14:00 LT, the PBL height lifted from ~0.5 km to ~0.6 km, while $\mathrm{PM}_{15–685\ \mathrm{nm}}$ decreased from ~24 μg m^{-3} to ~19 μg m^{-3} although there was a slight increase at the beginning of the period. This suggests the important effect of PBL evolution on $\mathrm{PM}_{15–685\ \mathrm{nm}}$. However, $N_{15–685\ \mathrm{nm}}$ sharply increased from ~7600 cm^{-3} at 07:00 LT to ~13000 cm^{-3} at 13:00 LT. This is related to the sudden burst of small Aitken mode particles (< 50 nm) when NPF events occurred. Newly formed fine particles contribute little to $\mathrm{PM}_{15–685\ \mathrm{nm}}$. In the evening, $\mathrm{PM}_{15–685\ \mathrm{nm}}$ increased gradually while $N_{15–685\ \mathrm{nm}}$ decreased. This is attributed to the declining trend in the nocturnal PBL and particle coagulation and growth. In other words, the evolution of the PBL played a dominant role on the aerosol mass concentration, while particle formation and growth had a greater influence on the variation in aerosol number concentration.

4.3.2. Diurnal variation in aerosol hygroscopicity

Figure 6c shows diurnal variations in κ_{gf} and κ_{chem}. All sized κ_{gf} increased beginning from the NPF event, especially for the 40 nm particles. The increase of κ_{gf} in the morning was synchronous with the particle number concentration ($N_{15–685\ \mathrm{nm}}$) but not with the PBL height, further suggesting the impact of photochemical reactions on aerosol hygroscopicity. The κ_{gf} for 40 nm particles increased from ~0.32 at 07:00 LT to ~0.44 at 15:00 LT, and approached the κ of pure ammonium sulfate, also suggesting that a large amount of hygroscopic compounds were produced during NPF events. Fig. S5 in the supplement shows the sharply increased concentrations of SO_2 and VOCs in the morning and the enhanced atmospheric oxidation capacity under high RH and low T made plenty of sulfate and SOA produced. This is the reason in the increase of aerosol hygroscopicity and the frequent occurrence of NPF events. Detailed characterization of aerosol chemistry during NPF events in this campaign has been studied in Zhang et al. (2018). The diurnal variation pattern in κ_{gf} for 80–200 nm particles differs from that of 40 nm particles. The differences in κ_{gf} between 80–200 nm particles in the early morning were large but gradually decrease as the sun rises. After 11:00 LT, the κ_{gf} for 80–200 nm particles were similar but lower than that of 40 nm particles. All these suggests the enhanced hygroscopicity in the 40–200 nm particles was likely caused by the condensation of sulfates and secondary organics (Fig. 6d) and the effect was more significant for 40 nm particles.

Figure 6c also shows that the κ_{chem} for PM_1 was lower than the κ_{gf} for 40–200 nm particles and had a weaker diurnal variation. This feature was stronger at noon when atmospheric oxidation and the aging process were more rapid. The difference was mainly induced by the simple ZSR mixing rule. During the daytime, the condensation of sulfuric acid on organics or BC greatly enhances their hygroscopicity (Zhang et al., 2008; Zhang et al., 2017). This phenomenon can't be described accurately by the ZSR model. Cruz and Pandis (2000) have shown that the measured κ_{gf} of internally mixed $(NH_4)_2SO_4$-organic aerosols is larger than the predicted κ_{chem} based on the ZSR model.

In summary, the ample supply of effluent SO_2 and VOCs provided sufficient precursors for the strong photochemical reactions at XT during this campaign, and the produce and condensation of sulfate and SOA enhanced aerosol hygroscopicity largely, especially during the daytime. This also suggests that the observed frequent NPF events were mainly induced by the oxidation of precursors.

4.3.3. Diurnal variation in CCN number concentration and activation ratio

Figure 7a shows the diurnal variations in N_{CCN} and AR at different SS. In the morning, N_{CCN} first decreased then increased while AR showed the opposite trend. This is related to the evolution of the PBL and NPF events. At the initial stage of an NPF event, the newly formed particles were less than 15 nm in size, which was below the detection limit of the SMPS. As a result, $N_{15\text{–}685\ \mathrm{nm}}$ decreased (Fig. 6b) as the PBL lifts and N_{CCN} also decreased. However, the mixing of aged particles within the PBL made the particle size (Fig. 7b) and AR increase slightly. With condensation and the growth of new particles, the number of fine particles detected by the SMPS increased rapidly but a portion of them cannot be activated because their smaller size. Therefore, N_{CCN} increased but AR decreased from 08:00 LT to 14:00 LT. In the afternoon and evening, N_{CCN} and AR increased slightly with the increase in particle size (Fig. 7b). However, these trends became weaker as SS decreased, this is because the critical diameter is larger at low SS and the influence of aerosol size distribution on N_{CCN} and AR is relatively weaker. This demonstrates that the particle size was the most important factor influencing the aerosol activation ability and the CCN number concentration, especially at larger SS levels. The sensitivity test of particle size in CCN closure study similar with that in Dusek et al. (2006) was shown in Fig. S6.

4.4. CCN estimation from chemical composition data

The three main factors influencing CCN activation are particle size, mixing state, and chemical composition. As discussed in the above sections, particles were highly internally mixed at XT and particle size had a great influence on N_{CCN}. In this section, a CCN closure study is conducted and the impact of chemical composition on N_{CCN} is discussed. Figure 8a shows estimated N_{CCN} as a function of measured N_{CCN} using real-time κ_{chem}. The estimated N_{CCN} correlates well with measurements ($R^2 \geqslant 0.85$) but is generally overestimated. The slope of each linearly fitted line is greater than 1.10 and increases with increasing SS. In addition, the relative deviation (RD) increases from 16.2 % to 25.2 % as SS increases from 0.13 % to 0.75 %, suggesting that estimates become worse at larger SS. The overestimation of N_{CCN} is mainly caused by large measurement uncertainties of CCNC: (1) the temperature or high flow rates in the CCNC may not allow enough time for particles to reach sizes large enough to be counted by the OPC at the exit of the CCN chamber (Lance et al., 2006; Cubison et al., 2008) and (2) in high particle number concentration environments, water depletion in the CCNC may reduce the counting rate of the CCNC (Deng et al., 2011). These uncertainties make measured N_{CCN} lower than the actual N_{CCN}. At larger SS, those activated aerosols in the cloud chamber of CCNC are greater in number and smaller in size, so the impact of these uncertainties is greater. The separated N_{CCN} closure study is shown in Fig. S7. Figure S7 suggests the CCN closure is very good when $N_{\mathrm{CCN}} < 5500\ \mathrm{cm}^{-3}$, reflecting the validation of the CCN closure method in this study.

Figure 8b shows estimated N_{CCN} using the mean value for κ_{chem} ($\kappa_{\mathrm{chem}} = 0.31$). Compared with results using real-time values for κ_{chem}, the fit parameters and RD change slightly, suggesting that the effect of chemical composition on N_{CCN} is weaker relative to the particle size. The sensitivity of estimated N_{CCN} to the variability in chemical composition (κ_{chem}) is further investigated (Fig. 9). In this figure, the variability of the equipotential lines in RD suggests that the sensitivity of N_{CCN} is strongly time dependent. This is attributed to the variability of the shape of the aerosol size distribution (Juranyi et al., 2010), further verifying the importance of particle size to N_{CCN}. The sensitivity of N_{CCN} to chemical composition (κ_{chem}) becomes weaker with increasing SS, suggesting that chemical composition becomes less important in N_{CCN} estimates at larger SS. In addition, the RD is always less than 10 % when estimating N_{CCN} using the mean value of κ_{chem}, suggesting that κ = 0.31 is a good proxy for chemical composition when estimating N_{CCN} at XT.

In summary, particle size is the most important factor influencing the aerosol activation ability at XT, especially at larger SS levels. The mixing state and chemical composition were not as important when estimating N_{CCN} because the particles were highly aged and internally mixed at XT, and aerosol hygroscopicity was not sensitive to estimates of N_{CCN}.

5. Summary and conclusions

The Atmosphere-Aerosol-Boundary Layer-Cloud (A^2BC) Interaction Joint Experiment was carried out at a suburban site located in the central North China Plain (NCP) from 1 May to 15 June of 2016. The aerosol hygroscopicity, mixing state and CCN activity at the site Xingtai (XT) were investigated in this study.

In general, the probability density function of the hygroscopicity parameter (κ-PDF) for 40–200 nm particles was a unimodal distribution, which is different from distributions at other sites in China. Particles of all sizes covered a large range of κ_{gf}

(mostly from 0 to 0.8) and showed similar κ-PDF patterns, suggesting that the hygroscopic compounds in these particles from 40 nm to 200 nm were similar at XT. The κ-PDF patterns also suggests that the particles were highly aged and internally mixed at XT during the this campaign. This is likely related to strong photochemical reactions.

The mean κ_{gf} for different particle sizes were larger in the daytime than at night. Daytime and nighttime κ_{gf} differences decreased with increasing particle size. This illustrates that the impact of photochemical reactions on aerosol hygroscopicity was strong and that the effect became weaker as particle sizes increases. The enhanced hygroscopicity of 40–200 nm particles was likely caused by the coating of sulfates or secondary organics and the effect was more significant for 40 nm particles. Compared with other sites in China, the aerosol hygroscopicity was much larger at XT because of the sufficient precursors and strong atmospheric oxidation capacity. The comparison also shows that the hygroscopicity of particles from different emissions and chemical processes differed largely.

New particle formation events occurred frequently at XT during this campaign. The evolution of the planetary boundary layer (PBL) played a dominant role on the aerosol mass concentration, while particle formation and growth had a greater influence on the variation in the aerosol number concentration. Particle size was the most important factor influencing the aerosol activation ability and the CCN number concentration at XT during the field experiment, especially at larger supersaturations (SS). Although the estimated N_{CCN} correlates well with measurements ($R^2 \geqslant 0.85$),

N_{CCN} is overestimated because of measurement uncertainties. The effect of chemical composition on N_{CCN} is weaker relative to the particle size. Sensitivity tests show that the impact of chemical composition on N_{CCN} becomes weaker as SS increases, suggesting that the effect of chemical composition on N_{CCN} estimates is less important at larger SS. The value $\kappa = 0.31$ is a good proxy for chemical composition when estimating N_{CCN} for the model at XT.

Our results show that aerosol properties in the middle of the NCP differ from those in the northern part of the NCP and other regions in China. This is because there are more industrial emissions in the central NCP. The plenitude of gas precursors and strong photochemical reactions at XT make aerosol properties there different from those at sites under other polluted conditions. More field measurements on gas-particle transformation and aerosol properties in this region are needed, which would be meaningful for studying the haze formation mechanism and climate change in the NCP.

Data availability. The data used in the study are available from the first author upon request (wang.yuying@mail.bnu.edu.cn).

Competing interests. The authors declare that they have no conflict of interest.

Author contribution. Z.L. and Y.W. designed the experiment, Y.W., Y.Z., and W.D. carried it out and analyzed the data, other co-authors participated in science discussions and suggested analyses. Y.W. prepared the manuscript with contributions from all co-authors.

Acknowledgements. This work was funded by the National Natural Science Foundation of China (NSFC) research projects (grant no. 91544217, 41675141, 41705125), the National Basic Research Program of China “973” (grant no. 2013CB955801), and the China Scholarship Council (award no. 201706040194). We also thank all participants in the field campaign for their tireless work and

cooperation.

References

Albrecht B.A.: Aerosols, Cloud Microphysics, and Fractional Cloudiness, Science, 245, 1227-30, 1989.

Brooks I.M.: Finding boundary layer top: Application of a wavelet covariance transform to lidar backscatter profiles, J. Atmos. Ocean. Tech., 20, 1092-1105, 2003.

Chu Y., Sauerwein M. and Chan C.K.: Hygroscopic and phase transition properties of alkyl aminium sulfates at low relative humidities, Phys. Chem. Chem. Phys., 17, 19789-19796, https://doi.org/10.1039/c5cp02404h, 2015.

Cohn S.A. and Angevine W.M.: Boundary layer height and entrainment zone thickness measured by lidars and wind-profiling radars, Journal of Applied Meteorology, 39, 1233-1247, 2000.

Covert D.S., Charlson R.J. and Ahlquist N.C.: A study of the relationship of chemical composition and humidity to light scattering by aerosols, Journal of Applied Meteorology, 11, 968-976, 1972.

Cruz C.N. and Pandis S.N.: Deliquescence and hygroscopic growth of mixed inorganic−organic atmospheric aerosol, Environ. Sci. Technol., 34, 4313-4319, https://doi.org/10.1021/es9907109, 2000.

Cubison M.J., Ervens B., Feingold G., Docherty K.S., Ulbrich I.M., Shields L., Prather K., Hering S. and Jimenez J.L.: The influence of chemical composition and mixing state of Los Angeles urban aerosol on CCN number and cloud properties, Atmos. Chem. Phys., 8, 5649-5667, https://doi.org/10.5194/acp-8-5649-2008, 2008.

Daniel R., Ulrike L., Raga G.B., O'Dowd C.D., Markku K., Sandro F., Anni R. and Andreae M.O.: Flood or drought: how do aerosols affect precipitation?, Science, 321, 1309-1313, https://doi.org/10.1126/science.1160606, 2008.

Deng Z.Z., Ma N., Liu P.F., Xu W.Y., Zhao C.S., Ran L., Chen J., Liang Z., Liang S. and Huang M.Y.: Size-resolved and bulk activation properties of aerosols in the North China Plain, Atmos. Chem. Phys., 11, 3835-3846, https://doi.org/10.5194/acp-11-3835-2011, 2011.

Dusek U., Frank G.P., Hildebrandt L., Curtius J., Schneider J., Walter S., Chand D., Drewnick F., Hings S. and Jung D.: Size matters more than chemistry for cloud-nucleating ability of aerosol particles, Science, 312, 1375-1378, https://doi.org/10.1126/science.1125261, 2006.

Eichler H., Cheng Y.F., Birmili W., Nowak A., Wiedensohler A., Brüggemann E., Gnauk T., Herrmann H., Althausen D. and Ansmann A.: Hygroscopic properties and extinction of aerosol particles at ambient relative humidity in South-Eastern China, Atmos Environ, 42, 6321-6334, https://doi.org/10.1016/j.atmosenv.2008.05.007, 2008.

Ervens B., Cubison M., Andrews E., Feingold G., Ogren J.A., Jimenez J.L., DeCarlo P. and Nenes A.: Prediction of cloud condensation nucleus number concentration using measurements of aerosol size distributions and composition and light scattering enhancement due to humidity, J. Geophys. Res.-Atmos., 112, https://doi.org/10.1029/2006JD007426, 2007.

Fu G.Q., Xu W.Y., Yang R.F., Li J.B. and Zhao C.S.: The distribution and trends of fog and haze in the North China Plain over the past 30 years, Atmos. Chem. Phys., 14, 11949-11958, https://doi.org/10.5194/acp-14-11949-2014, 2014.

Gomez-Hernandez M., McKeown M., Secrest J., Marrero-Ortiz W., Lavi A., Rudich Y., Collins D.R. and Zhang R.: Hygroscopic Characteristics of Alkylaminium Carboxylate Aerosols, Environ. Sci. Technol., 50, 2292-2300, https://dx.doi.org/10.1021/acs.est.5b04691, 2016.

Guo S., Hu M., Lin Y., Gomez-Hernandez M., Zamora M.L., Peng J., Collins D.R. and Zhang R.:

OH-Initiated Oxidation of m-Xylene on Black Carbon Aging, Environ. Sci. Technol., 50, 8605-8612, https://dx.doi.org/10.1021/acs.est.6b01272, 2016.

Gysel M., Crosier J., Topping D.O., Whitehead J.D., Bower K.N., Cubison M.J., Williams P.I., Flynn M.J., McFiggans G.B. and Coe H.: Closure study between chemical composition and hygroscopic growth of aerosol particles during TORCH2, Atmos. Chem. Phys., 7, 6131-6144, https://doi.org/10.5194/acp-7-6131-2007, 2007.

Huang R., Zhang Y., Bozzetti C., Ho K., Cao J., Han Y., Daellenbach K.R., Slowik J.G., Platt S.M., Canonaco F., Zotter P., Wolf R., Pieber S.M., Bruns E.A., Crippa M., Ciarelli G., Piazzalunga A., Schwikowski M., Abbaszade G., Schnelle-Kreis J., Zimmermann R., An Z., Szidat S., Baltensperger U., Haddad I.E. and Prévôt A.S.H.: High secondary aerosol contribution to particulate pollution during haze events in China, Nature, https://doi.org/10.1038/nature13774, 2014.

IPCC: Climate change 2013: Scientific basis, Fifth assessment of the Inter-governmental Panel on Climate Change, Cambridge University Press, 2013.

Jacobson M.C., Hansson H.C., Noone K.J. and Charlson R.J.: Organic atmospheric aerosols: Review and state of the science, Rev. Geophys., 38, 267-294, https://doi.org/10.1029/1998RG000045, 2000.

Jiang R.X., Tan H.B., Tang L.L., Cai M.F., Yin Y., Li F., Liu L., Xu H.B., Chan P.W., Deng X.J. and Wu D.: Comparison of aerosol hygroscopicity and mixing state between winter and summer seasons in Pearl River Delta region, China, Atmos. Res., 169, 160-170, https://doi.org/10.1016/j.atmosres.2015.09.031, 2016.

Jimenez J.L., Canagaratna M.R., Donahue N.M., Prevot A., Zhang Q., Kroll J.H., DeCarlo P.F., Allan J.D., Coe H. and Ng N.L.: Evolution of organic aerosols in the atmosphere, Science, 326, 1525-1529, https://doi.org/10.1126/science.1180353, 2009.

Juranyi Z., Gysel M., Weingartner E., DeCarlo P.F., Kammermann L. and Baltensperger U.: Measured and modelled cloud condensation nuclei number concentration at the high alpine site Jungfraujoch, Atmos. Chem. Phys., 10, 7891-7906, https://doi.org/10.5194/acp-10-7891-2010, 2010.

Köhler H.: The nucleus in and the growth of hygroscopic droplets, Transactions of the Faraday Society, 32, 1152-1161, 1936.

Kulmala M., Petäjä T., Nieminen T., Sipilä M., Manninen H.E., Lehtipalo K., Dal Maso M., Aalto P.P., Junninen H. and Paasonen P.: Measurement of the nucleation of atmospheric aerosol particles, Nat. Protoc., 7, 1651-1667, https://doi.org/10.1038/nprot.2012.091,2012.

Lance S., Nenes A., Medina J. and Smith J.N.: Mapping the operation of the DMT continuous flow CCN counter, Aerosol Sci. Tech., 40, 242-254, http://dx.doi.org/10.1080/02786820500543290, 2006.

Lebo Z.J., Shipway B.J., Fan J., Geresdi I., Hill A., Miltenberger A., Morrison H., Rosenberg P., Varble A. and Xue L.: Challenges for cloud modeling in the context of aerosol-cloud-precipitation interactions, B. Am. Meteorol. Soc., https://doi.org/10.1175/BAMS-D-16-0291.1, 2017.

Li Y., Zhang F., Li Z., Sun L., Wang Z., Li P., Sun Y., Ren J., Wang Y. and Cribb M.: Influences of aerosol physiochemical properties and new particle formation on CCN activity from observation at a suburban site of China, Atmos. Res., 188, 80-89, https://doi.org/10.1016/j.atmosres.2017.01.009, 2017.

Li Z., Lau W.M., Ramanathan V., Wu G., Ding Y., Manoj M.G., Liu J., Qian Y., Li J. and Zhou T.: Aerosol and monsoon climate interactions over Asia, Rev. Geophys., https://doi.org/10.1002/2015RG000500, 2016.

Li Z., Daniel R. and Fan J.W.: Aerosols and Their Impact on Radiation, Clouds, Precipitation, and

Severe Weather Events, Oxford Research Encyclopedias: Environmental science, https://doi.org/10.1093/acrefore/9780199389414.013.126, 2017.

Liu P.F., Zhao C.S., Bel T.G., Hallbauer E., Nowak A., Ran L., Xu W.Y., Deng Z.Z., Ma N., Mildenberger K., Henning S., Stratmann F. and Wiedensohler A.: Hygroscopic properties of aerosol particles at high relative humidity and their diurnal variations in the North China Plain, Atmos. Chem. Phys., https://doi.org/10.5194/acp-11-3479-2011, 2011.

Lopez-Yglesias X.F., Yeung M.C., Dey S.E., Brechtel F.J. and Chan C.K.: Performance Evaluation of the Brechtel Mfg. Humidified Tandem Differential Mobility Analyzer (BMI HTDMA) for Studying Hygroscopic Properties of Aerosol Particles, Aerosol Sci Tech, 48, 969-980, http://dx.doi.org/10.1080/02786826.2014.952366, 2014.

Meng J.W., Yeung M.C., Li Y.J., Lee B.Y.L. and Chan C.K.: Size-resolved cloud condensation nuclei (CCN) activity and closure analysis at the HKUST Supersite in Hong Kong, Atmos. Chem. Phys., 14, 10267-10282, https://doi.org/10.5194/acp-14-10267-2014, 2014.

Ng N.L., Herndon S.C., Trimborn A., Canagaratna M.R., Croteau P.L., Onasch T.B., Sueper D., Worsnop D.R., Zhang Q. and Sun Y.L.: An Aerosol Chemical Speciation Monitor (ACSM) for routine monitoring of the composition and mass concentrations of ambient aerosol, Aerosol Sci. Tech., 45, 780-794, http://dx.doi.org/10.1080/02786826.2011.560211, 2011.

Peng J., Hu M., Guo S., Du Z., Zheng J., Shang D., Zamora M.L., Zeng L., Shao M. and Wu Y.: Markedly enhanced absorption and direct radiative forcing of black carbon under polluted urban environments, Proceedings of the National Academy of Sciences, 113, 4266-4271, https://doi.org/10.1073/pnas.1602310113, 2016.

Petters M.D. and Kreidenweis S.M.: A single parameter representation of hygroscopic growth and cloud condensation nucleus activity, Atmos. Chem. Phys., 7, 1961-1971, https://doi.org/10.5194/acp-7-1961-2007, 2007.

Qiu C. and Zhang R.: Physiochemical Properties of Alkylaminium Sulfates: Hygroscopicity, Thermostability, and Density, Environ. Sci. Technol., 46, 4474-4480, https://dx.doi.org/10.1021/es3004377, 2012.

Quan J., Gao Y., Zhang Q., Tie X., Cao J., Han S., Meng J., Chen P. and Zhao D.: Evolution of planetary boundary layer under different weather conditions, and its impact on aerosol concentrations, Particuology, 11, 34-40, https://doi.org/10.1016/j.partic.2012.04.005, 2013.

Ramanathan V., Crutzen P.J., Kiehl J.T. and Rosenfeld D.: Aerosols, climate, and the hydrological cycle, Science, 294, 2119-2124, https://doi.org/10.1126/science.1064034, 2001.

Rose D., Gunthe S.S., Mikhailov E., Frank G.P., Dusek U., Andreae M.O. and Pöschl U.: Calibration and measurement uncertainties of a continuous-flow cloud condensation nuclei counter (DMT-CCNC): CCN activation of ammonium sulfate and sodium chloride aerosol particles in theory and experiment, Atmos. Chem. Phys., 8, 1153-1179, https://doi.org/10.5194/acp-8-1153-2008, 2008.

Schmale J., Henning S., Decesari S., Henzing B., Keskinen H., Sellegri K., Ovadnevaite J., Pöhlker M.L., Brito J., Bougiatioti A., Kristensson A., Kalivitis N., Stavroulas I., Carbone S., Jefferson A., Park M., Schlag P., Iwamoto Y., Aalto P., Äijälä M., Bukowiecki N., Ehn M., Frank G., Fröhlich R., Frumau A., Herrmann E., Herrmann H., Holzinger R., Kos G., Kulmala M., Mihalopoulos N., Nenes A., O'Dowd C., Petäjä T., Picard D., Pöhlker C., Pöschl U., Poulain L., Prévôt A.S.H., Swietlicki E., Andreae M.O., Artaxo P., Wiedensohler A., Ogren J., Matsuki A., Yum S.S., Stratmann F., Baltensperger U. and Gysel M.: Long-term cloud condensation nuclei number concentration, particle number size distribution and chemical composition measurements at regionally representative observatories, Atmos Chem Phys, 18, 2853-2881, https://doi.org/10.5194/acp-18-2853-2018, 2018.

Stock M., Cheng Y.F., Birmili W., Massling A., Wehner B., Müller T., Leinert S., Kalivitis N., Mihalopoulos N. and Wiedensohler A.: Hygroscopic properties of atmospheric aerosol particles over the Eastern Mediterranean: implications for regional direct radiative forcing under clean and polluted conditions, Atmos. Chem. Phys., 11, 4251-4271, https://doi.org/10.5194/acp-11-4251-2011, 2011.

Stokes R.H. and Robinson R.A.: Interactions in aqueous nonelectrolyte solutions. I. Solute-solvent equilibria, The Journal of Physical Chemistry, 70, 2126-2131, 1966.

Stolzenburg M.R. and McMurry P.H.: Equations governing single and tandem DMA configurations and a new lognormal approximation to the transfer function, Aerosol Sci. Tech., 42, 421-432, http://dx.doi.org/10.1080/02786820802157823, 2008.

Stolzenburg M.R. and McMurry P.H.: TDMAFIT user's manual, University of Minnesota, Department of Mechanical Engineering, Particle Technology Laboratory, Minneapolis, 1-61, 1988.

Sun Y., Wang Z., Dong H., Yang T., Li J., Pan X., Chen P. and Jayne J.T.: Characterization of summer organic and inorganic aerosols in Beijing, China with an Aerosol Chemical Speciation Monitor, Atmos. Environ., 51, 250-259, https://doi.org/10.1016/j.atmosenv.2012.01.013, 2012.

Swietlicki E., Hansson H.C., HÄMeri K., Svenningsson B., Massling A., McFiggans G., McMurry P.H., PetÄJÄ T., Tunved P., Gysel M., Topping D., Weingartner E., Baltensperger U., Rissler J., Wiedensohler A. and Kulmala M.: Hygroscopic properties of submicrometer atmospheric aerosol particles measured with H-TDMA instruments in various environments—a review, Tellus B, 60, 432-469, https://doi.org/10.1111/j.1600-0889.2008.00350.x, 2008.

Tan H., Xu H., Wan Q., Li F., Deng X., Chan P.W., Xia D. and Yin Y.: Design and application of an unattended multifunctional H-TDMA system, J. Atmos. Ocean. Tech., 30, 1136-1148, https://doi.org/10.1175/JTECH-D-12-00129.1, 2013.

Tritscher T., Juranyi Z., Martin M., Chirico R., Gysel M., Heringa M.F., DeCarlo P.F., Sierau B., Prevot A.S.H., Weingartner E. and Baltensperger U.: Changes of hygroscopicity and morphology during ageing of diesel soot, Environ. Res. Lett., 6, https://doi.org/10.1088/1748-9326/6/3/034026, 2011.

Twomey S.: Pollution and the planetary albedo, Atmos. Environ., 8, 1251-1256, 1974.

Ulbrich I.M., Canagaratna M.R., Zhang Q., Worsnop D.R. and Jimenez J.L.: Interpretation of organic components from Positive Matrix Factorization of aerosol mass spectrometric data, Atmos. Chem. Phys., 9, 2891-2918, https://doi.org/10.5194/acp-9-2891-2009, 2009.

Wang L.T., Wei Z., Yang J., Zhang Y., Zhang F.F., Su J., Meng C.C. and Zhang Q.: The 2013 severe haze over southern Hebei, China: model evaluation, source apportionment, and policy implications, Atmos. Chem. Phys., 14, 3151-3173, https://doi.org/10.5194/acp-14-3151-2014, 2014.

Wang Y., Zhang F., Li Z., Tan H., Xu H., Ren J., Zhao J., Du W. and Sun Y.: Enhanced hydrophobicity and volatility of submicron aerosols under severe emission control conditions in Beijing, Atmos. Chem. Phys., 17, 5239-5251, https://doi.org/10.5194/acp-17-5239-2017, 2017.

Wang Z., Wu Z., Yue D., Shang D., Guo S., Sun J., Ding A., Wang L., Jiang J. and Guo H.: New particle formation in China: Current knowledge and further directions, Sci. Total Environ., 577, 258-266, https://doi.org/10.1016/j.scitotenv.2016.10.177, 2017.

Wu Z.J., Zheng J., Shang D.J., Du Z.F., Wu Y.S., Zeng L.M., Wiedensohler A. and Hu M.: Particle hygroscopicity and its link to chemical composition in the urban atmosphere of Beijing, China, during summertime, Atmos. Chem. Phys., 16, 1123-1138, https://doi.org/10.5194/acp-16-1123-2016, 2016.

Ye X., Tang C., Yin Z., Chen J., Ma Z., Kong L., Yang X., Gao W. and Geng F.: Hygroscopic growth of urban aerosol particles during the 2009 Mirage-Shanghai Campaign, Atmos. Environ., 64, 263-269, https://doi.org/10.1016/j.atmosenv.2012.09.064, 2013.

Zhang F., Li Y., Li Z., Sun L., Li R., Zhao C., Wang P., Sun Y., Liu X., Li J., Li P., Ren G. and Fan T.: Aerosol hygroscopicity and cloud condensation nuclei activity during the AC^{3}Exp campaign: implications for cloud condensation nuclei parameterization, Atmos. Chem. Phys., 14, 13423-13437, https://doi.org/10.5194/acp-14-13423-2014, 2014.

Zhang F., Li Z., Li Y., Sun Y., Wang Z., Li P., Sun L., Wang P., Cribb M., Zhao C., Fan T., Yang X. and Wang Q.: Impacts of organic aerosols and its oxidation level on CCN activity from measurement at a suburban site in China, Atmos. Chem. Phys., 16, 5413-5425, https://doi.org/10.5194/acp-16-5413-2016, 2016.

Zhang F., Wang Y., Peng J., Ren J., Collins D., Zhang R., Sun Y., Yang X. and Li Z.: Uncertainty in predicting CCN activity of aged and primary aerosols, J. Geophys. Res.-Atmos., 122, https://doi.org/10.1002/2017JD027058, 2017.

Zhang Y., Du W., Wang Y., Wang Q., Wang H., Zheng H., Zhang F., Shi H., Bian Y., Han Y., Fu P., Canonaco F., Prévôt A.S.H., Zhu T., Wang P., Li Z. and Sun Y.: Aerosol chemistry and particle growth events at an urban downwind site in the North China Plain, Atmos. Chem. Phys. Discuss., 2018, 1-29, https://doi.org/10.5194/acp-2017-889, 2018.

Zhang R., Khalizov A.F., Pagels J., Zhang D., Xue H. and McMurry P.H.: Variability in morphology, hygroscopicity, and optical properties of soot aerosols during atmospheric processing, Proceedings of the National Academy of Sciences, 105, 10291-10296, https://doi.org/10.1073/pnas.0804860105,2008.

Zhang R., Wang L., Khalizov A.F., Zhao J., Zheng J., McGraw R.L. and Molina L.T.: Formation of nanoparticles of blue haze enhanced by anthropogenic pollution, Proceedings of the National Academy of Sciences, 106, 17650-17654, https://doi.org/10.1073/pnas.0910125106, 2009.

Zhang S.L., Ma N., Kecorius S., Wang P.C., Hu M., Wang Z.B., Größ J., Wu Z.J. and Wiedensohler A.: Mixing state of atmospheric particles over the North China Plain, Atmos. Environ., 125, Part A, 152-164, https://doi.org/10.1016/j.atmosenv.2015.10.053, 2016.

Zhu Y., Zhang J., Wang J., Chen W., Han Y., Ye C., Li Y., Liu J., Zeng L., Wu Y., Wang X., Wang W., Chen J. and Zhu T.: Distribution and sources of air pollutants in the North China Plain based on on-road mobile measurements, Atmos. Chem. Phys., 16, 12551-12565, https://doi.org/10.5194/acp-16-12551-2016, 2016.

Table 1. The number fractions of different hygroscopic groups for different particle sizes.

	40 nm	80 nm	110 nm	150 nm	200 nm
NH	5.1 %	5.0 %	5.1 %	5.0 %	5.7 %
LH	4.8 %	4.2 %	4.3 %	4.7 %	5.1 %
MH	90.1 %	90.8 %	90.6 %	90.3 %	89.2 %

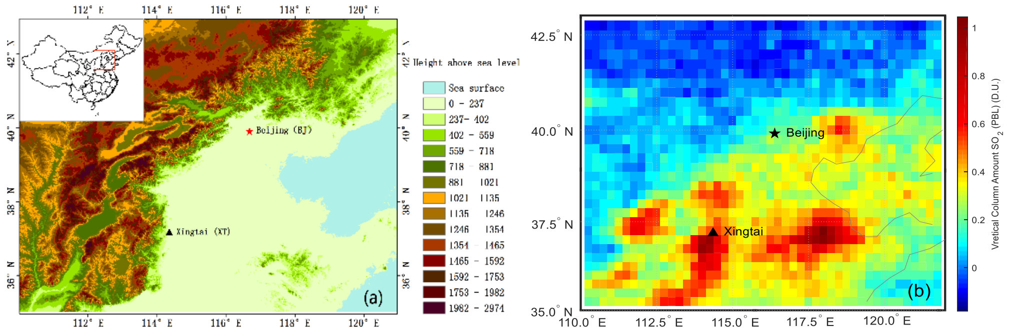

Figure 1. (**a**) Map showing the location of the sampling site and (**b**) the distribution of mean SO$_2$ concentrations of May from 2012 to 2016.

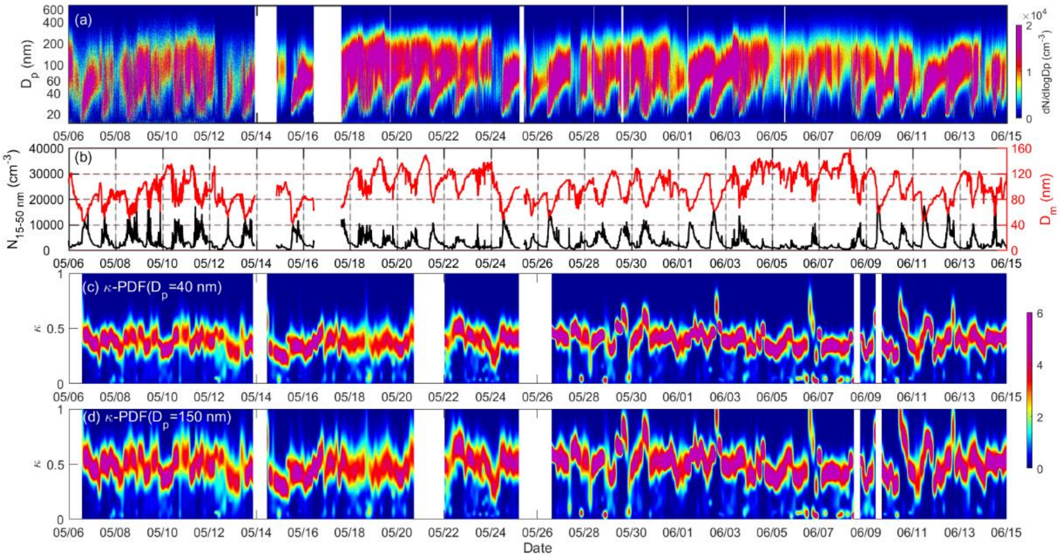

Figure 2. The time series of (**a**) particle number size distribution (PNSD), (**b**) aerosol number concentration in the 15–50 nm range ($N_{15\text{–}50\ \mathrm{nm}}$) and the geometric mean diameter (D_m), (**c**) the probability density function of κ_gf (κ-PDF) for 40 nm and (**d**) 150 nm particles from 6 May to 15 June of 2016.

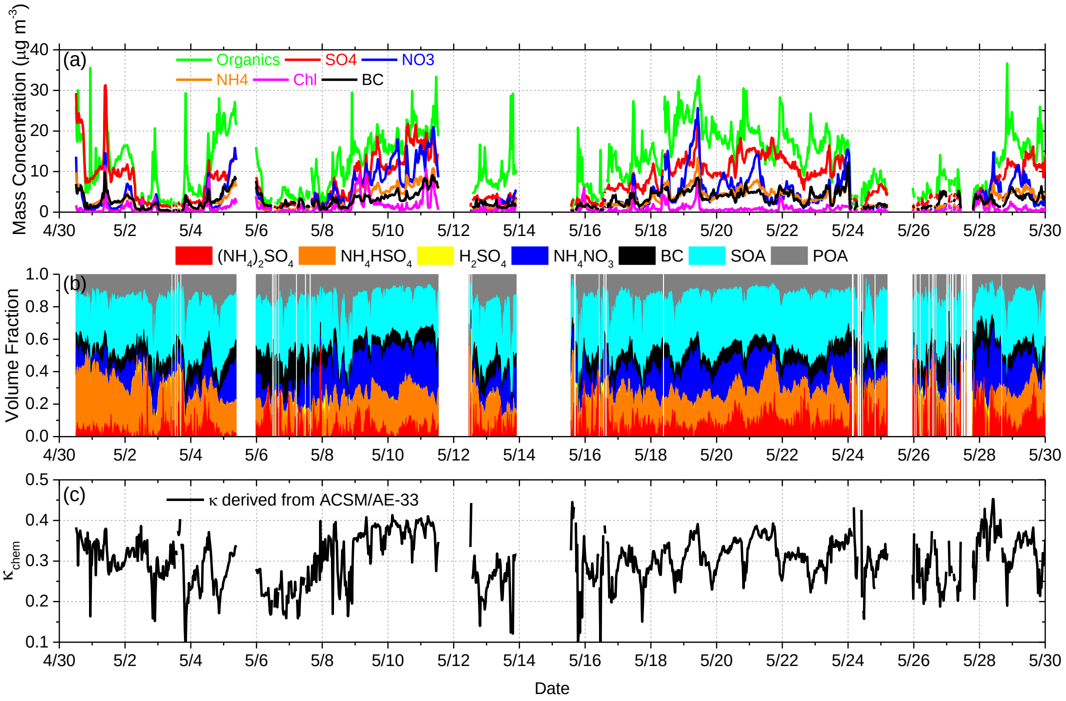

Figure 3. Time series of (**a**) the bulk mass concentration of aerosol species in PM_1, (**b**) the volume fractions of POA, SOA, BC, and inorganics with the simplified ion pairing scheme, and (**c**) the hygroscopicity parameter derived from the chemical compositions (κ_{chem}).

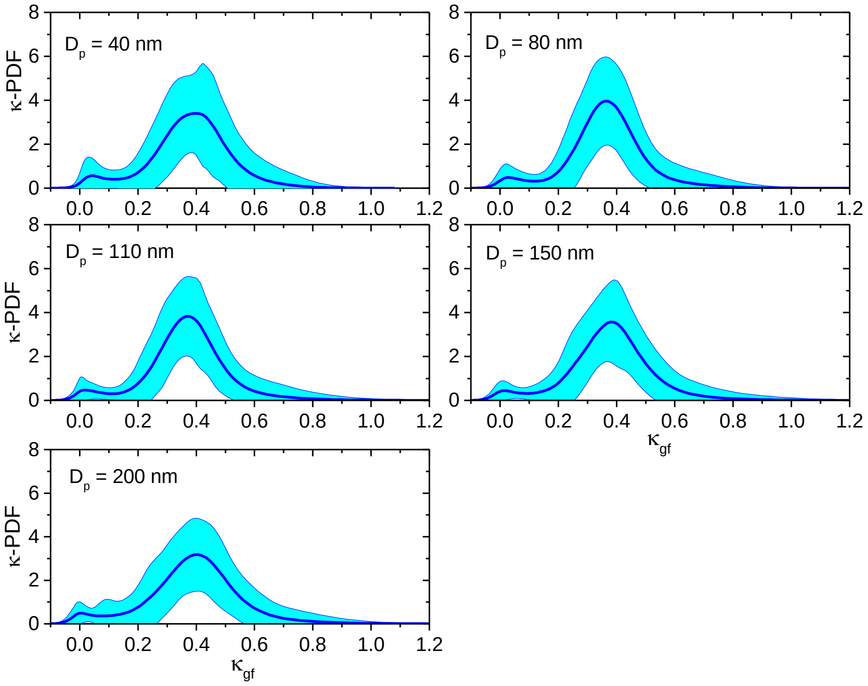

Figure 4. Mean probability density functions of κ_{gf} (κ-PDF) for different particle sizes and their standard deviations (shaded areas) derived from H-TDMA data and measured at RH = 85 %.

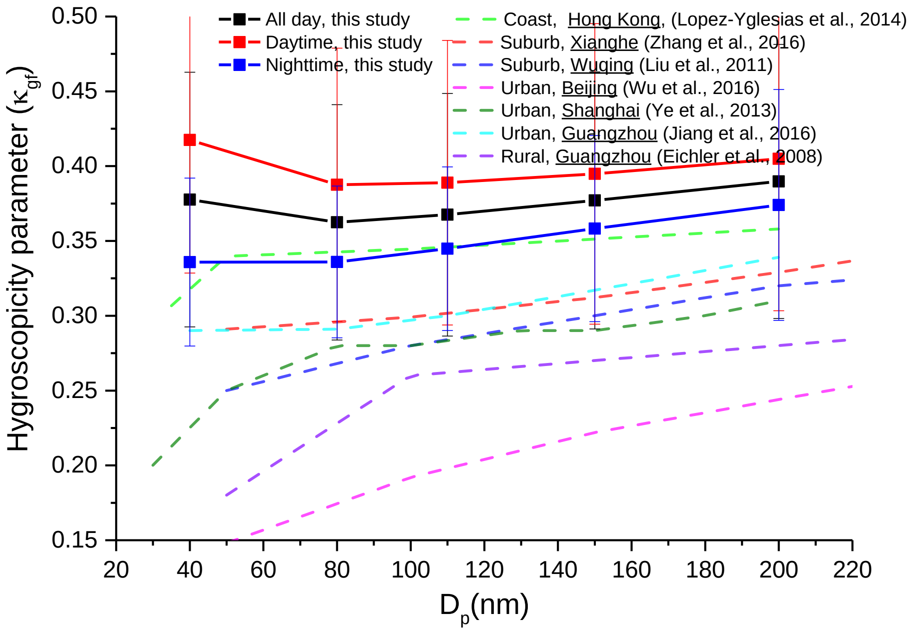

Figure 5. Size-resolved aerosol hygroscopicity parameter (κ_{gf}) derived from H-TDMA data at XT and at other sites in China.

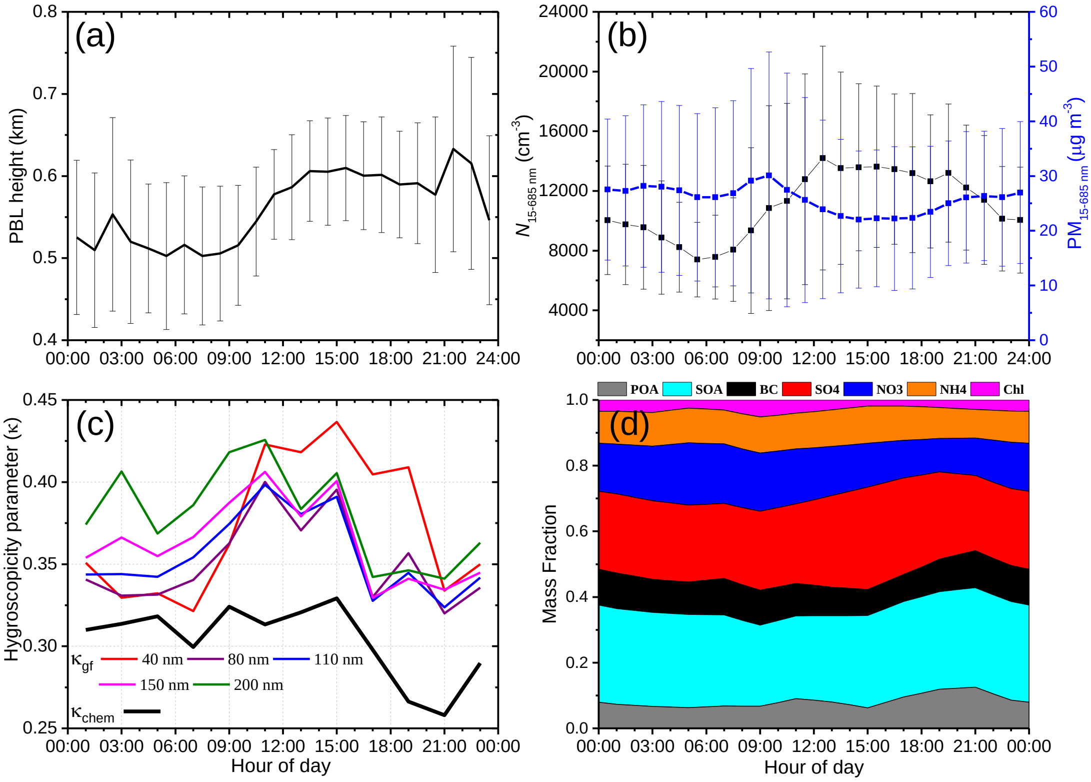

Figure 6. Diurnal variations in (**a**) planetary boundary layer (PBL) height retrieved from the MPL, (**b**) aerosol number and mass concentrations in the 15–685 nm range ($N_{15\text{–}685\ \mathrm{nm}}$ and $\mathrm{PM}_{15\text{–}685\ \mathrm{nm}}$, respectively) derived from the SMPS (an aerosol density of 1.6 g cm^{-3} is assumed), (**c**) the hygroscopicity parameter derived from the hygroscopic growth factor (κ_{gf}) and predicted from the bulk chemical composition (κ_{chem}), and (**d**) the mass fractions of different species.

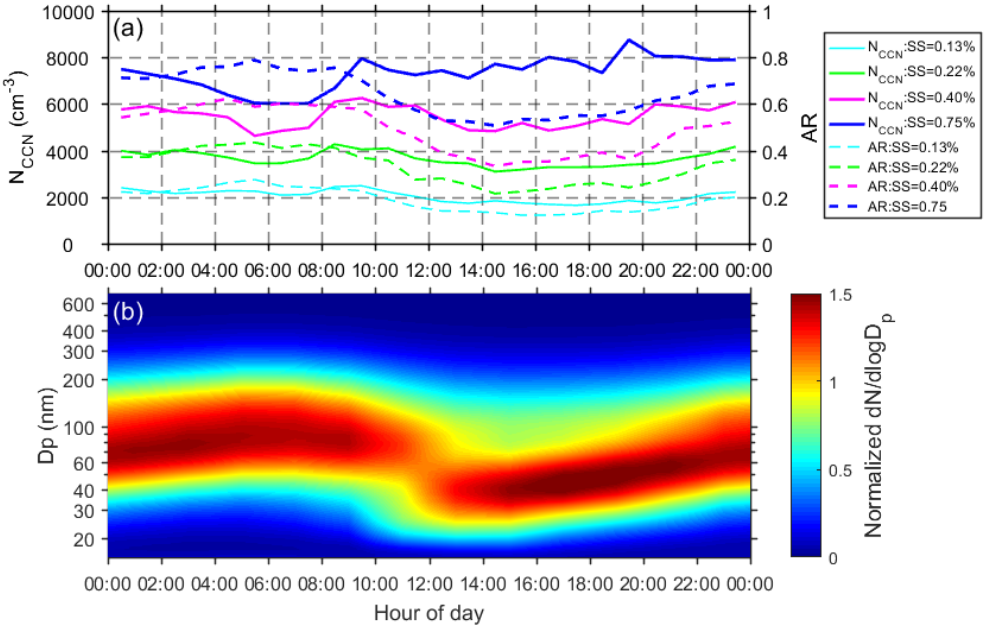

Figure 7. Diurnal variations in (a) CCN number concentration (N_{CCN}) and activation ratio (AR), and (b) the normalized aerosol size distribution in the 15–685 nm particle size range.

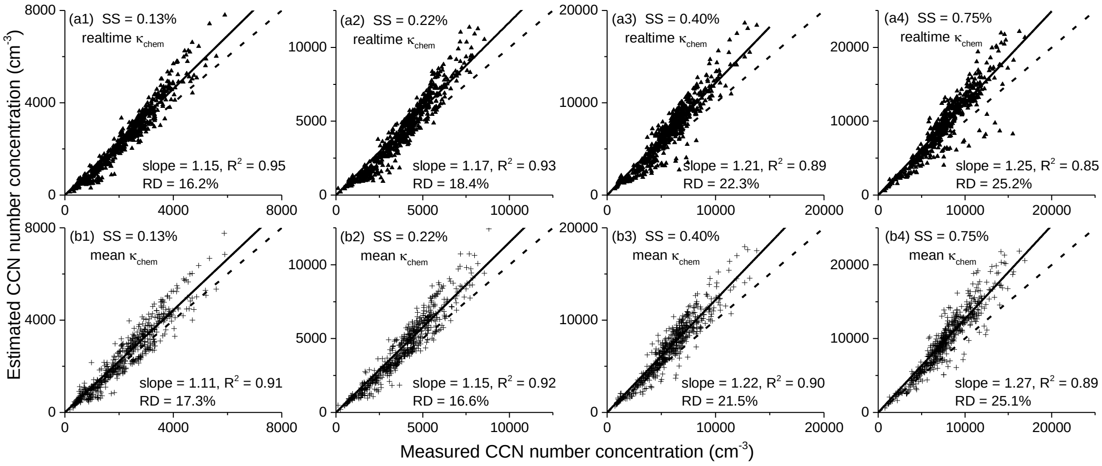

Figure 8. Estimated versus measured CCN number concentration for ambient aerosols at four different supersaturation levels. The N_{CCN} is estimated based on κ-Köhler theory, using the real-time κ_{chem} (**a1-a4**) and the mean κ_{chem} (**b1-b4**). The slope and correlation coefficient (R^2) of the linear regression, and the relative

deviation of estimated N_{CCN} (RD = $|N_{\mathrm{CCN\_estimated}} - N_{\mathrm{CCN\_measured}}| / N_{\mathrm{CCN\_measured}}$) are shown in each panel. The regression line is overlaid on the measurements (solid line) and the dashed line is the 1:1 line.

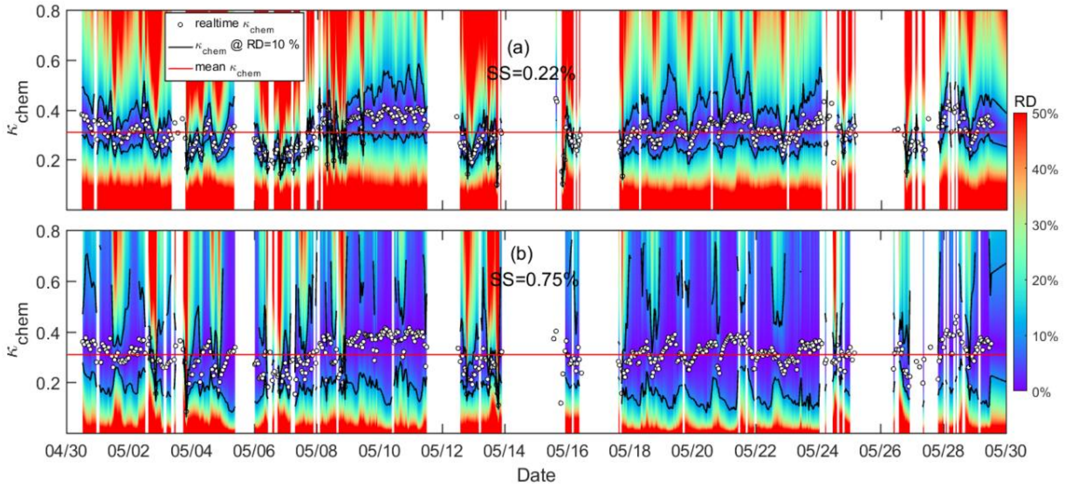

Figure 9. Sensitivity of N_{CCN} estimates to κ_{chem} as a function of time at (a) SS = 0.22 % and (b) SS = 0.75 %. The color scale indicates the relative deviation (RD) of the CCN estimates using the κ_{chem} value shown on the ordinate. In each panel, open circles show the real-time κ_{chem}. Note that RD is by definition zero at these points. The black line is κ at RD = 10 % and the red line is the mean value for κ_{chem} (0.31). Figure S8 in the supplement shows the same plots but for SS = 0.13 % and 0.40 %.